ELSEVIER

Journal of Alloys and Compounds 330–332 (2002) 476–482

Journal of ALLOYS AND COMPOUNDS

www.elsevier.com/locate/jallcom

Hydriding kinetics analysis by the frequency response method. Application to the ZrNi–H_2(g) system

P. Millet, P. Dantzer*

CNRS-UMR 8647, Bât 415, Université Paris Sud, 91405 Orsay Cedex, France

Abstract

Hydrogen absorption–desorption reactions in the ZrNi–H_2(g) system were carried out with high-precision calorimeter-volumetric devices specifically devoted to simultaneous thermodynamic and kinetic analysis. Strict control of the experimental parameters ensures quasi-isothermal conditions during the phase transformation. The effect of the operating temperature in the range 400–500 K and the activation process on the kinetics of phase transformation was studied. Time-domain analysis of the kinetics was performed using an empirical rate law based on a nucleation and growth mechanism. Up to 500 K, the fit of the experimental kinetics is satisfactory. However, differences remain between the measured and calculated curves, especially in the early stages of the transformation. To demonstrate evidence for a possible surface rate limitation, the kinetics were then analyzed in the frequency domain using the frequency response method (FRM). It is shown that the high-frequency shape of the transfer function plotted in Nyquist coordinates consists of a semi-circle located along the real axis, the diameter of which is directly related to the operating temperature and correlated with the activation process. The present possibilities and limitations of the FRM are discussed. © 2002 Elsevier Science B.V. All rights reserved.

Keywords: Hydriding kinetics analysis; Frequency response method

1. Introduction

This work is concerned with the kinetic analysis of hydride phase growth in the ZrNi–H_2(g) system, which can potentially be used for hydrogen isotope storage or separation technology [1,2] or in closed-cycle hydride cryo-coolers [3]. Whereas structural and thermodynamic studies of this system have been carried out [4–10], the hydriding and dehydriding kinetics of ZrNi has received little attention. This field deserves special attention from both an applied and a fundamental viewpoint. For practical applications, kinetic rate constants are needed for design purposes. For fundamental considerations, a detailed analysis of the kinetics provides information on the mechanisms of phase transformation, and on the effect of the experimental conditions on the mechanisms. This is of paramount importance for controlling hydride phase growth/decomposition and for achieving a large number of absorption/desorption cycles [11].

Whereas time-domain analysis of kinetic data is commonly used to assess the validity of model rate laws, it may be desirable to perform the analysis in the frequency domain using the frequency response method (FRM). Interest in using the FRM over conventional time-domain analysis is clearly established. Although its use requires mathematical manipulations, an immediate benefit comes from the fact that, in favorable cases, the kinetic features of each step of a multi-step reaction mechanism appear at different frequencies. Identification of the various steps of the mechanism is therefore made easier. The applicability of the FRM to solid–gas reactions has been successfully demonstrated in the study of sorption phenomena [12] and for analyzing hydrogen absorption (desorption) by (from) intermetallic compounds (IMC) in the solid solution domain [13]. From a general viewpoint, the FRM is aimed at determining the transfer function of a system for different frequencies of interest. The most popular method is to apply an harmonically varying input and collect the associated response. Experimentally, however, the production of well-shaped harmonic pressure perturbations is not a simple task and frequency-rich signals of various shape can be used as an alternative. The determination of the transfer function will be restricted to the frequency content of the perturbating signal. Another limitation related to the use of sine-like perturbations is that the system must behave linearly. If this condition is not satisfied as for a first-order phase transformation accom-

*Corresponding author.

E-mail address: pierre.dantzer@lemhe.u-psud.fr (P. Dantzer).

0925-8388/02/$ – see front matter © 2002 Elsevier Science B.V. All rights reserved.
PII: S0925-8388(01)01652-8

panied by hysteresis, the applicability of the FRM imposes drastic constraints, especially on the shape of the perturbating signal. It can be shown experimentally that as long as the perturbation respects a criterion of directionality ($d(H/M)/dt > 0$ for absorption or $d(H/M)/dt < 0$ for desorption), there exists a linear relationship between the excitation and the response. The system is linear by parts, i.e. behaves linearly as long as the perturbation respects the criterion of directionality [14]. Thus, by using such signals, it is possible to obtain a transfer function similar to that obtained for a true and complete linear system, except that a restriction is imposed on its use. Such transfer functions can be used, for example, to predict the response of the system if and only if the perturbation respects the criterion of directionality. Otherwise, the prediction will be erroneous. Conversely, the transfer function can be used to recover the true shape of a perturbating signal if and only if the response shows that the criterion of directionality is respected. The FRM is used in this article for analyzing the kinetics of the phase transformation associated with the formation/decomposition of compound $ZrNiH_{3-\delta}$ from the monohydride ZrNiH.

2. Experimental procedure

The experimental setup used in this work was specifically developed for simultaneous thermodynamic and kinetic studies. A detailed description is given in Ref. [14]. Results related to the thermodynamic and calorimetric analysis of the ZrNi–H_2(g) system have been published in Refs. [10,15]. Kinetic data were obtained as follows. H_2 is transferred during the absorption process from a reference volume chamber (V_1) to the reactor (V_2) with typical changes in composition $\delta H/M = 0.03$ (each experiment lasted for 2 h). The driving force for the transfer comes from the initial difference of pressure between V_1 and V_2. During the desorption process, the residual pressure in the reference volume chamber is pumped down to vacuum and H_2 is transferred back from the reactor to the chamber. The needle valve located between V_1 and V_2 is used to slow down the hydrogen mass flow so that the transformation remains quasi-isothermal ($|\Delta T| < 0.5$°C). The time-dependent pressures in the reference volume chamber $P_1(t)$ and in the reactor $P_2(t)$ provide the raw data for the kinetic analysis. Typical results obtained during absorption at 116.3°C are shown in Fig. 1. Details of the experimental series obtained for two different batches of ZrNi (samples 1 and 2) are compiled in Table 1. Sample 1 intentionally contains traces of cerium oxide to make it brittle. Sample 2 is an ingot of very high purity.

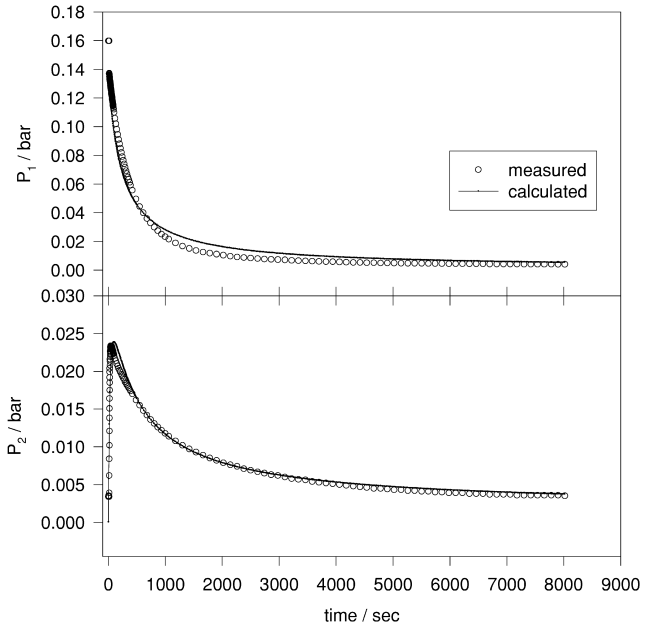

Fig. 1. Measured (○) and calculated (———) values of (a) $P_1(t)$ and (b) $P_2(t)$ during hydrogen absorption at 116.3°C; $H/M = 1.889$.

Table 1
Identification of the series with the thermodynamic paths followed during the processes of absorption and desorption

Series	T (°C)	Abs.	Des.	Evacuation, annealing	H/M
Sample 1	81.0	*Activation*		●	0.00→2.80
1	116.3	●		●	0.00→2.74
2	126.6	●			0.00→2.74
3	126.6		●		2.74→2.64
4	152.6		●	●	2.64→2.53
5	152.9	●			0.00→2.66
6	191.2		●		2.66→2.02
7	191.1	●			2.02→2.58
Sample 2	83.4	*Activation*			0→0.05
8	210.6	*Activation*			0.05→2.52
9	210.6		●		2.52→1.43
10	210.6	●		●	1.43→2.51
11	226.1	●			0→2.46
12	226.1		●		2.46→0.92
13	226.1	●			0.92→2.45

3. Kinetic analysis in the time domain

3.1. Description of the model

It has been shown elsewhere [16] that the mass flow of a gas through a needle valve obeys Poiseuille's law. Assuming that, at operating pressures (<5 bar), hydrogen behaves ideally, the time-dependent pressures $P_1(t)$ and $P_2(t)$ are the solutions of [16]

$$\left.\frac{dP_1}{dt}\right|_t = \frac{K_{NV}}{V_1}[P_1^2(t) - P_2^2(t)] \quad (1)$$

$$\left.\frac{dP_2}{dt}\right|_t = \frac{K_{NV}}{V_2}[P_1^2(t) - P_2^2(t)] \quad (2)$$

where K_{NV} is a constant characterizing the geometry of the needle valve and the viscosity of the gas at the operating temperature.

The model rate law used to fit the kinetics comes from the theory of isothermal transformations in metals and alloys developed by Johnson and Mehl [17] and Avrami [18–20]. Based on a mechanism of nucleation and growth, the theory provides a general rate equation which accounts for different growth mechanisms:

$$\alpha(t) = 1 - \exp(-kt^n) \quad (3)$$

where α is the transformed fraction of the sample, k is the rate constant and n is a constant characterizing the shape of the growing phase. α and k are defined as

$$\alpha = \left(\frac{H}{M}\bigg|_t - \frac{H}{M}\bigg|_{\text{init}}\right) \Big/ \left(\frac{H}{M}\bigg|_{\text{final}} - \frac{H}{M}\bigg|_{\text{init}}\right) \quad (4)$$

$$k = k_0 \cdot \exp\left[\frac{-E}{RT}\right] \quad (5)$$

Derivation of Eq. (3) yields the rate of phase transformation $d\alpha/dt$ at the temperature of the transformation. To produce the hydride phase transformation, an overpressure must be applied to the sample. The driving force of the transformation is taken into account in the rate law by adding the pressure term $[P_2(t) - P_{eq}]$, where $P_2(t)$ is the actual pressure of the gas phase and P_{eq} is the plateau 'equilibrium' pressure associated with the composition $(H/M)|_t$. Finally, the rate law takes the form proposed by Goodell and Rudman [21]:

$$\frac{d\alpha}{dt} = k \cdot [P_2(t) - P_{eq}(t)] \cdot [1 - \alpha(t)] \cdot t^{(n-1)} \cdot n \quad (6)$$

3.2. Results and discussion

The solutions to the model $P_1(t)$ and $P_2(t)$ are obtained by solving Eqs. (1), (2) and (6) with the appropriate boundary conditions using a finite difference method. k and n are the two only adjustable parameters. The best correlations between measured and calculated pressure curves were obtained numerically using the non-linear least-square routine of Levenberg-Marquardt [22] (Fig. 1). The agreement between measured and calculated pressure curves supports the validity of the model. However, some differences exist, especially in the early stages of the transformation, suggesting a possible different rate determining step such as H chemisorption. Since multi-step mechanisms are not easily modeled in the time domain, this possibility will be treated in detail by analyzing the kinetics in the frequency domain (see below).

Fig. 2a and b show the values of k and n corresponding to the best fit of $P_1(t)$ and $P_2(t)$ obtained for the different series of Table 1. Whereas a small discrepancy is observed for the morphological factor n, the value of the kinetic constant k can be directly related to the temperature and to the activation/annealing history of the sample, as can be

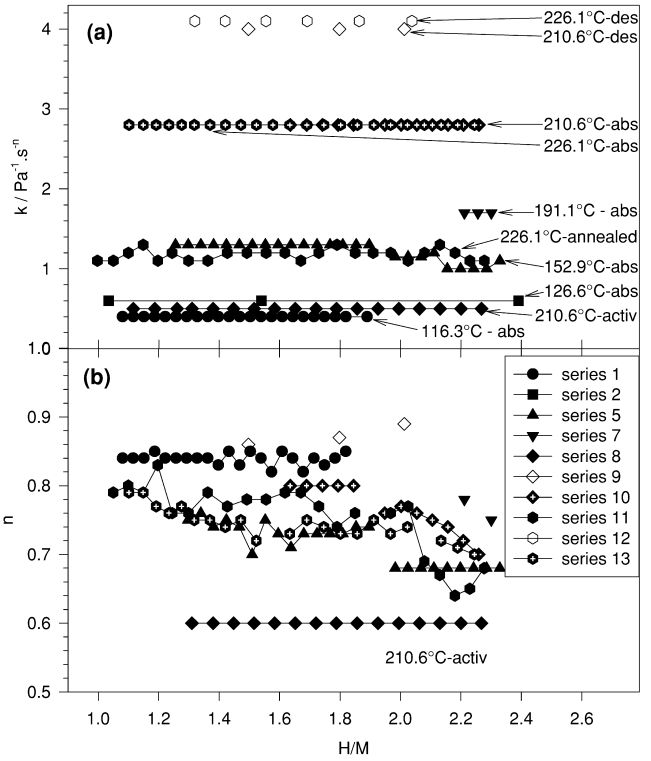

Fig. 2. Effect of the operating temperature and the activation process on (a) the rate constant k of the JMA rate law and (b) the morphological parameter.

seen from Fig. 2a. For each series, the values of k is independent of the composition, indicating that reproducible kinetics are observed all over the composition domain for each increment of hydrogen. This in turn means that the rigorous experimental conditions used in this work are appropriate for studying the kinetic behavior.

For the activated sample (series 1, 2, 5, 7, 10 and 13), an Arrhenius activation rate law can be derived for the temperature domain under consideration:

$$\text{Ln}\, k = -3380.3*1/T + 7.925 \quad (400\ \text{K} < T < 500\ \text{K})$$

where k is expressed in ($\text{Pa}^{-1}\ \text{s}^{-n}$) and T is in Kelvin.

The role of the activation process was followed through series 8 to 10. Series 8 corresponds to the activation process of the sample. Although the experiment was conducted at 210.6°C, the value of k (0.5) is close to that obtained at 116.3°C for an already activated sample. As expected, the kinetics of the first absorption series is low. In the two subsequent series (9, desorption and 10, absorption), the value of k is higher (4.0 and 2.8, respectively), indicating a desorption process faster than the absorption process, and a faster kinetics for the second absorption scan. This last observation is consistent with the fact that the initially massive sample becomes finely divided after the first absorption series. The growing hydride phases generate defects in the material and the

subsequent absorption series are made easier and proceed faster.

The role of the annealing treatment was followed through series 11 to 13 at 226.1°C. At the end of series 10, the sample was de-hydrided under vacuum at 350°C. The following absorption series (11), corresponding to the annealed sample, gives $k = 1.1$, which is higher than the value obtained for the unactivated sample (series 8) but lower than the value obtained at 226.1°C during the second absorption scan (series 13). Again, the value of k obtained during the desorption process (series 12) is higher than for the absorption process of the activated sample (series 13).

From these results it can be concluded that, using a nucleation and growth rate law, the effect of the operating temperature, and of the activation and annealing processes, on the kinetics can be followed in the time domain through variation of the rate constant k. It is not possible, however, to conclude the type of rate limiting process, although a value of n close to unity is typical of a process controlled by grain boundary nucleation after saturation.

4. Kinetic analysis in the frequency domain

4.1. Experimental transfer functions

By analogy with electrical impedance which relates the electric potential perturbation to the resulting current, the transfer function associated with a solid–gas reaction will relate, in the frequency domain, the perturbation applied to the system (ex. a pressure or chemical potential modulation) to the resulting gaseous mass flow. The experimental transfer functions are obtained directly from the time-dependent pressures $P_1(t)$ and $P_2(t)$ recorded in the reference volume chamber and in the reactor during each experiment. From Eq. (1) or (2), the following expression for the time-dependent hydrogen mass flow, dn_{H_2}/dt, can be obtained:

$$\frac{dn_{H_2}}{dt}(t) = \frac{K_{NV}}{RT}[P_1^2(t) - P_2^2(t)] \quad (7)$$

The global transfer functions $Z_T(\omega)$ are obtained by taking the ratio of the Fourier transform of $P_2(t)$ to the Fourier transform of dn_{H_2}/dt. The graph of $Z_T(\omega)$ is plotted either in the form of a Nyquist diagram (real vs. imaginary part for different values of the frequency) or in the form of a Bode diagram (phase and amplitude are plotted separately vs. the frequency on a log scale). Although calculation of the discrete Fourier transform of raw data is routine using either a fast Fourier transform (FFT) or a discrete Fourier transform algorithm (DFT) [22], obtaining the correct transfer functions is non-trivial. The most frequently encountered problem in using the discrete Fourier transform is aliasing, a term which refers to the fact that high-frequency components of a time function impersonate low frequencies if the sampling rate is too low [23]. The answer to this problem involves the sampling of the time function at a rate at least twice as high as the highest frequency (Nyquist criterion) or passing the signal through a low-pass filter. A typical sampling rate of one measure/s is required over the 2 h of each experiment.

Experimental transfer functions obtained at 226.1°C for the $\beta \rightarrow \gamma$ phase transformation are plotted in Fig. 3 as a function of the composition H/M.

4.2. Model transfer functions

The model transfer function which describes hydrogen transfer from the reference volume chamber to the reactor through the needle valve can be constructed from the following considerations. In the absence of a sample in the reactor, hydrogen flows to the reactor across the needle valve, which acts as a 'pneumatic resistance'. In the empty reactor, the gas accumulates, increasing the pressure until the driving force across the needle valve falls to zero. The free volume part of the reactor acts as a 'pneumatic capacitor' where gaseous hydrogen can be stored. In the presence of a sample, the gas which enters the reactor can either accumulate in the free volume part of the reactor or react with the sample. To account for this possible alternative, an equivalent electrical circuit is used in which the pneumatic capacitor of the reactor is connected in parallel to the transfer function of the gas-absorbing sample. The case where hydrogen dissolves in the sample to form a solid solution has been treated elsewhere [13]. It was shown that the transfer function associated with the sample consisted of two terms connected in series, corre-

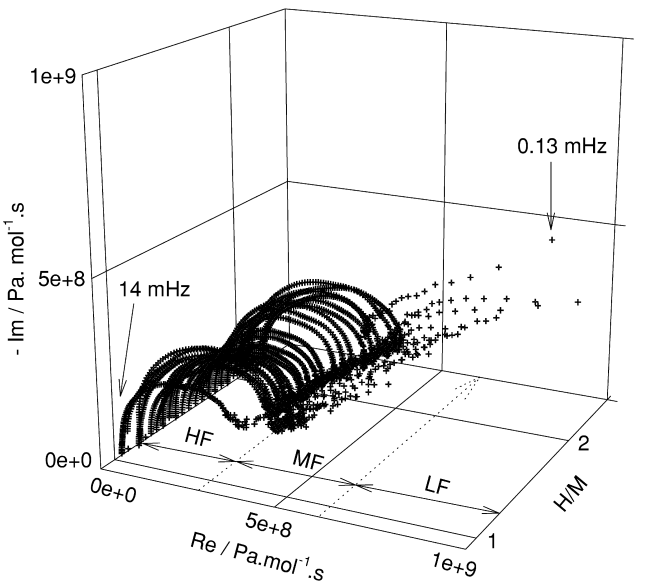

Fig. 3. Experimental transfer functions obtained as a function of H/M during absorption at 226.1°C. HF, MF and LF: high-, medium- and low-frequency domains.

sponding to hydrogen surface chemisorption followed by diffusion-limited absorption into the bulk sample.

To account for the phase transformation, we still assume the existence of a two-step reaction scheme consisting of: (i) hydrogen surface chemisorption, followed by (ii) nucleation and growth phase transformation. H transport from the surface to the growing nuclei of the hydride phase is assumed to be a fast process. The equivalent circuit of this reaction mechanism is shown in Fig. 4. The expression of the impedance Z_n associated with the nucleation and growth mechanism has been studied in detail elsewhere [24]. It was shown that, whereas at high frequency Z_n tends to zero, at lower frequencies Z_n is equivalent to a RC circuit connected in series. The resistance is denoted R_n and the capacitance C_S. In the low-frequency domain, R_n is a function of the reciprocal of k and C_S [24]. Since in these IMC–H_2 systems C_S is high, and since at the operating temperatures k is also high, the value of R_n is low. Thus the impedance Z_n reduces to C_S and the graph of the transfer function is quite different depending on whether the surface resistance is zero or not. This is shown in Fig. 5 for $n \approx 0.8$, a value obtained for ZrNi–H from data analysis in the time domain. As R_s increases, a semi-circle develops along the real axis. This is the signature of surface resistance, the value of which is given by the diameter of the semi-circle.

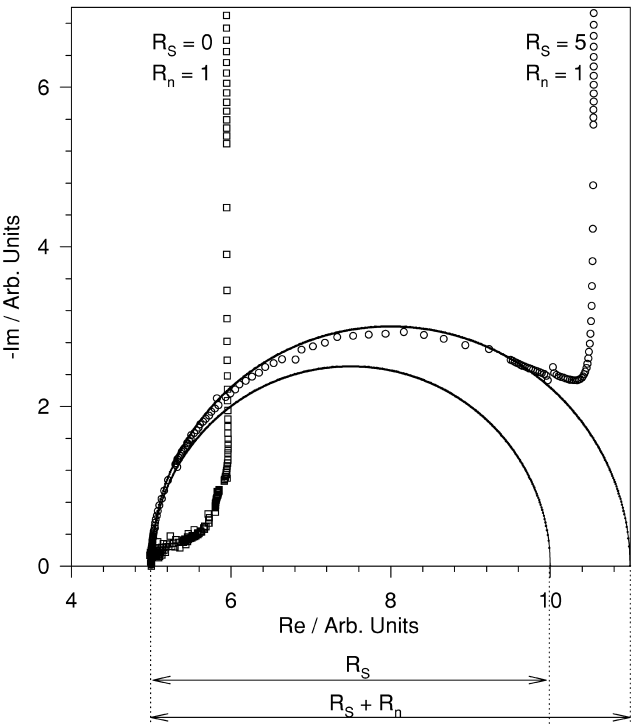

Fig. 5. Calculated transfer function diagrams of the equivalent circuit of Fig. 4 showing the role of the surface resistance R_s. $k = 1$; $n = 0.8$.

4.3. Data analysis and discussion

As can be seen from Fig. 3, the experimental transfer functions consist essentially of a high-frequency semi-circle located along the real axis of the Nyquist diagram. This is the signature of a resistance connected in parallel to the pneumatic capacitor of the free volume part of the reactor as discussed above. A comparison with the model transfer function of Fig. 5 leads to the conclusion that there exists a hydrogen chemisorption step in the global mechanism of phase transformation. Thus, analysis of the kinetics with the FRM provides direct information on surface phenomena. It becomes possible to follow surface modifications such as real surface changes during the activation or annealing processes, surface blocking by partial oxidation or pollutant adsorption, etc.

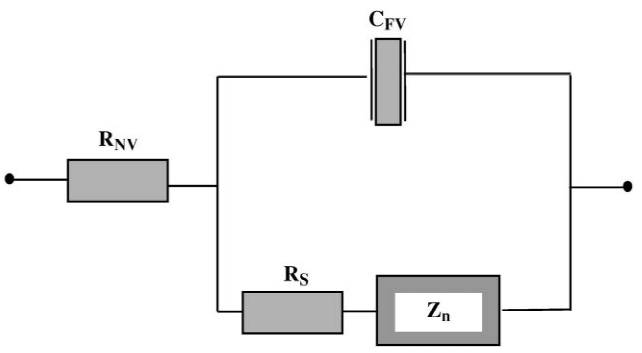

Fig. 4. Model equivalent electric circuit used to analyze the experimental transfer functions. R_{NV}, needle valve resistance; C_{FV}, free volume capacitance; R_S, surface resistance; Z_n, impedance associated with the nucleation and growth mechanism for different values of the morphological parameter n.

The role of the operating temperature and of the state of activation of the sample on the value of the surface resistance for the series of Table 1 is shown in Fig. 6. For a fully activated sample (series 1 and 5), the surface resistance decreases upon increasing the operating temperature, as expected. For a non-activated sample (series 8), the values of the surface resistance during the first hydriding cycle is significantly higher. This is followed by a rapid decrease by a factor of 10 during the second absorption cycle (series 10). This change may be related to the modification of the sample surface as a result of the first hydriding cycle. This observation also holds true, but to a lesser extent, for the sample annealed at high temperature (series 11). This observation illustrates the effect of defect on the kinetics.

4.4. Limitations of the FRM

The use of the FRM for studying the mechanism of phase transformation in solid–gas reactions has several limitations. Except for the problems related to the rate of sampling as discussed above and the problems related to the precision of the measured pressures and mass flow, the choice of the appropriate form of the perturbating pressure

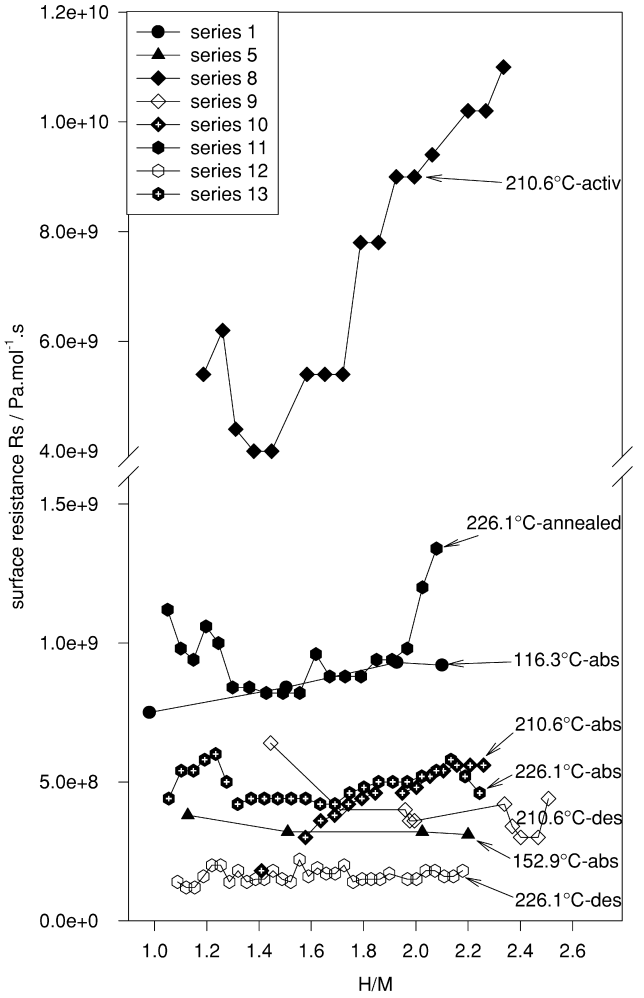

Fig. 6. Plot of the experimental diameter of the high-frequency semi-circle as a function of composition. Role of the operating temperature and activation process.

modulation is of great importance. It can be seen from Fig. 3 that the medium frequency does not appear clearly on the experimental transfer functions and that the low-frequency capacitive behavior which is expected is not observed. This comes from two factors, which are correlated. First, the hydrogen absorption capacitance C_s is substantially high. Since the impedance of a capacitor varies with the reciprocal of its capacitance, low-frequency capacitive behavior can be observed only at low frequencies, i.e. by waiting a sufficiently long time (several hours for the total transformation of ZrNiH into $ZrNiH_{3-\delta}$). But, and this is the second factor, to fulfill our goal of controlling the growth of the hydride phase, we use an experimental setup designed so that the driving force which causes the hydrogen mass flow to the reactor and fuels the reaction falls to zero in ca. 1.5 h. Consequently, the hydrogen mass flow falls to zero, not because of the limited absorbing capacitance of the sample, but because the perturbation itself falls to zero. These two factors explain why the low-frequency behavior of the experimental transfer functions is truncated.

Application of the FRM to the study of phase transformations in solid–gas reactions still requires further experimental improvements to increase the precision and the bandwidth of the transfer functions. By using more appropriate pressure perturbations, the medium- and low-frequency domains should become accessible.

5. Conclusion

In this study, the kinetics of the $\beta \rightarrow \gamma$ phase transformation in the ZrNi–H_2(g) system was analyzed in the temperature range 400–500 K. Data analysis in the time domain using a classical nucleation and growth rate law provides satisfactory fits except for the early stages of the transformation, where a possible kinetic limitation by surface hydrogen chemisorption is suspected. Data analysis was then conducted in the frequency domain for which experimental transfer functions can be obtained. These transfer functions reveal a characteristic high-frequency semi-circle which is interpreted as the signature of surface rate-controlling hydrogen chemisorption. The value of the diameter of the semi-circle gives the value of the surface resistance. A correlation is observed between the value of the resistance and (i) the operating temperature, with an increased temperature yielding a lower resistance, and (ii) the activation of the sample, with the first hydrogen absorption cycle yielding substantially higher resistances which rapidly decrease in the subsequent absorption/desorption cycles. This observation is related to the formation of a fine sample powder of increasing specific surface as the absorption/desorption cycles proceed.

References

[1] K. Watanabe, K. Tanaka, M. Matsuyama, K. Hasegawa, Fusion Eng. Design 18 (1991) 27.
[2] N. Mitsuishi, S. Fukada, N. Tanimura, J. Less-Common Met. 123 (1986) 65.
[3] R.C. Bowman, P.B. Karlmann, S. Bard, Brilliant Eyes Ten-Kelvin Sorption Cryocooler Experiment (BETSCE), Final Report, JPL Publication 97-14, 1997.
[4] G.G. Libowitz, H.F. Hayes, T.R.P. Gibb, J. Phys. Chem. 62 (1958) 76.
[5] M.E. Kost, L.N. Padurets, A.A. Chertkov, V.I. Mikheeva, Russ. J. Inorg. Chem. 25 (1980) 471, translated from Zh. Neorg. Khim. 25 (1980) 847.
[6] D.G. Westlake, H. Shaked, P.R. Mason, B.R. McCart, M.H. Mueller, J. Less-Common Met. 88 (1982) 17.
[7] W. Luo, A. Craft, T. Kuji, H.S. Chung, T.B. Flanagan, J. Less-Common Met. 162 (1990) 251.
[8] I.E. Nemirovskaya, A.M. Alekseev, V.V. Lunin, J. Alloys Comp. 177 (1991) 1.
[9] R. Kronski, T. Schober, J. Alloys Comp. 205 (1994) 175.
[10] P. Dantzer, P. Millet, T.B. Flanagan, Met. Mater. Trans. 32A (2001) 29.

[11] P. Dantzer, M. Pons, A. Guillot, Z. Phys. Chem. 183 (1994) 205.
[12] L.M. Naphtali, L.M. Polinski, J. Phys. Chem. 67 (1963) 369.
[13] P. Millet, P. Dantzer, J. Alloys Comp. 253 (1997) 542.
[14] P. Dantzer, P. Millet, Rev. Sci. Instr. 71 (2000) 142.
[15] P. Dantzer, P. Millet, Thermochim. Acta 370 (2001) 1.
[16] H.Y. Caï, P. Millet, P. Dantzer, J. Alloys Comp. 231 (1995) 427.
[17] W.A. Johnson, R.F. Mehl, Trans. Am. Inst. Min. (Metall.) Eng. 135 (1939) 416.
[18] M. Avrami, J. Chem. Phys. 7 (1939) 1103.
[19] M. Avrami, J. Chem. Phys. 8 (1940) 212.
[20] M. Avrami, J. Chem. Phys. 9 (1941) 177.
[21] P.D. Goodell, P.S. Rudman, J. Less-Common Met. 89 (1983) 117.
[22] W.H. Press, B.P. Flannery, S.A. Teukolsky, W.H. Vetterling, Numerical Recipes: The Art of Scientific Computing, Cambridge University Press, 1986.
[23] G.D. Bergland, IEEE spectrum, July 1969, p. 41.
[24] P. Millet, P. Dantzer, Electrochem. Commun. 1 (1999) 163.